Time Scales in Polymer Electrophoresis through Narrow Constrictions: A Brownian Dynamics Study

Ajay S. Panwar and Satish Kumar*

Department of Chemical Engineering and Materials Science, University of Minnesota, 151 Amundson Hall, 421 Washington Ave. SE, Minneapolis, Minnesota 55455

Received May 20, 2005; Revised Manuscript Received November 28, 2005

ABSTRACT: Brownian dynamics simulations are used to characterize the time scales involved in polymer electrophoresis through narrow constrictions. The polymer is modeled as a freely jointed bead−rod chain with a total charge distributed uniformly among the beads. The narrow constriction is a thin channel with height $h_s < R_g$ which separates two thicker channels, both of height $h_l \sim R_g$ where R_g is the polymer radius of gyration. The polymer is initially placed in a thick channel, and an applied electric field drives it into the next thick channel through the intervening narrow constriction. We find that the electrophoresis of the polymer is characterized by three time scales, each of which depends on the polymer chain length, N. An approach time, τ_{app}, describes the motion of the polymer to the entrance of the thin channel. Upon reaching the entrance of the thin channel, the polymer is entropically trapped, and its escape from the trap is associated with an activation time, τ_{act}. After the activation event, the motion of the polymer through the thin channel and into the next thick channel is characterized by a crossing time, τ_{cross}. We find that whereas τ_{app} and τ_{act} decrease with N, τ_{cross} increases with N. As a consequence, it is found that the transit velocity of the polymer, $v_{transit}$, first increases with N and then decreases beyond a certain value of N. The position of the maximum in $v_{transit}$ is shown to depend on the applied electric field strength, the relative values of h_s and h_l, and whether the channel is two-dimensional or three-dimensional. We discuss the relevance of this behavior to polymer electrophoresis in microfluidic channels exhibiting entropic trapping effects and polymer translocation through nanopores.

1. Introduction

The transport of a polymer molecule through a narrow constriction is associated with an energy barrier arising from loss of configurational entropy inside the constriction. Such processes are commonly observed in electrophoretic separations of DNA in sieving media such as gels or microfluidic channels,[1,2] and in translocation of DNA or RNA through nanopores in nuclear and cellular membranes.[3,4] To move across the narrow constriction, the polymer first has to surmount the energy barrier to enter the constriction, and then all of its segments must move through the constriction and ultimately out of it. Both processes can be characterized by time scales which generally depend on the polymer chain length, N. A knowledge of the relevant time scales and their dependence on chain length, and variables such as the geometry of the constriction and the strength of the applied electric field, can help in designing better separation techniques for biopolymers and also provide insight into the mechanisms of macromolecular transport in biological systems.

Han and Craighead[5−8] studied the electrophoretic motion of DNA molecules in a microfluidic device which consisted of alternating thick and thin channels (Figure 1). The depth of the thick channels was comparable to the radius of gyration, R_g, of the DNA, whereas the depth of the thin channels was much smaller than R_g. The application of an electric field forces the DNA to move into the thin channels, but loss of entropy inside the thin channels presents an entropic barrier to its motion. The DNA was found to remain trapped at the entrance of the thin channel for an amount of time which depends on chain length. A surprising and seemingly counterintuitive observation was that DNA mobility increased with chain length. The authors explained this observation by arguing that the longer DNA molecules are able to escape into the thin channel faster because they present more segments at the entrance of the thin channel, and this facilitates the DNA escape. The motion of the DNA from one thick channel to the next, through the intervening thin channel, can be described by a transit time which can be used to extract a transit velocity or a mobility for the DNA. Thus, the transit time for a DNA molecule in this device is found to depend on the time for which it is trapped at the entrance of the thin channel. Since the trapping time decreases with N, the transit velocity is found to increase with N.

In a pioneering experiment, Kasianowicz and co-workers[9] studied the motion of DNA driven through a nanopore by an externally applied electric field. The nanopore was an artificially created protein channel with an internal diameter of about 2 nm. They found that the time for which the channel is blocked by the DNA increases with chain length. Since that time is the same as the time it takes for the DNA to move through the nanopore, the transit time increases with N and the transit velocity decreases with N.

The entropic trapping and nanopore experiments display opposite dependences of the transit velocity on N, indicating that the time scales which govern the transit velocity in each experiment represent different physical mechanisms of polymer transport. The trapping time in the entropic trapping experiments represents the time required to surmount an energy barrier,[5] and the blockade time in the nanopore experiments corresponds to the time required to ensure that all segments of the polymer have passed through the pore.[9,10] In both experiments, the polymer first has to overcome an energy barrier at the entrance of the constriction, and then all of its segments must move through the constriction. However, the results of each experiment suggest that only one of these processes is manifested in the nature of the observed transit times. This implies that under the conditions used for these experiments the time scales corresponding to the two processes are so far separated from each other that only one of them determines the behavior of the transit velocity.

10.1021/ma051041o CCC: $33.50
Published on Web 01/11/2006

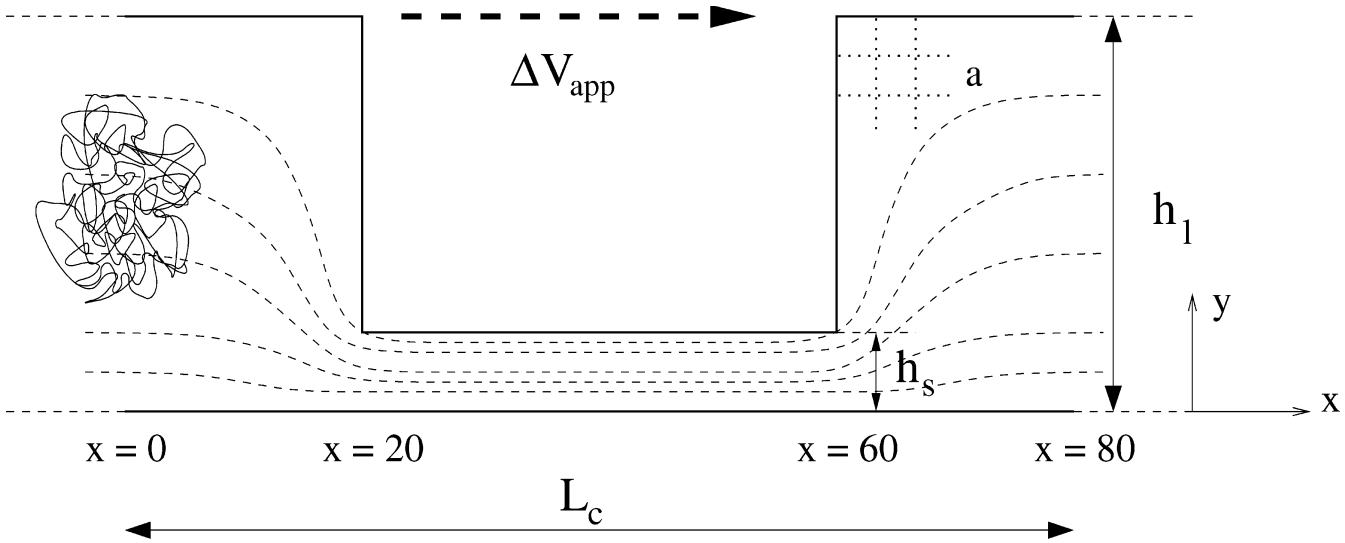

Figure 1. A schematic of the model geometry used in the simulations. The length of the channel, L_c, represents the pitch length of the entropic trapping device and is repeated along x to get a series of entropic traps separated by entropic barriers. The thick channels, with a height h_l, serve as entropic traps for the charged polymer chain. The thin channels, with a height h_s, are the narrow constrictions through which the polymer must traverse in order to move from one entropic trap to another. The size of the polymer is such that $h_l \sim R_g$, but $h_s < R_g$ so that the polymer faces an entropic barrier at the entrance of the thin channel. The driving force for the polymer is an externally applied potential difference, ΔV_{app}. The grid size in the finite-difference calculations is denoted by a.

There have been many previous studies—experimental,[5−15] analytical,[16−28] and computational[29−42]—on polymer electrophoresis through a narrow constriction. Two of these are particularly relevant to the present paper. In an analytical study, Muthukumar[24] considered the translocation of a polymer through a nanopore to be comprised of three stages, each with a characteristic time scale. All three time scales were found to depend on pore length, and as a result, the total translocation time displayed a nonmonotonic dependence on the pore length. However, only one of the three time scales was found to depend on N. Although the dependence of translocation time on chain length was not discussed, the results suggest that the translocation time would increase with N. Chen[35] has used Monte Carlo simulations to study the driven translocation of a polymer through a nanopore, where translocation was assumed to consist of two steps. The first involves a chain end finding its way into the nanopore (activation), and the second involves the movement of the chain through the nanopore (crossing). Although the chain length dependence of these time scales was calculated for different applied potential gradients, their relative importance and interaction were not studied. Hence, it is not immediately clear how the transit velocity would behave as a function of chain length under conditions where the two time scales—related to activation and crossing—become comparable to each other. In general, one might expect that the transit velocity of the polymer would depend on an interplay between these different time scales.

In the present study, we examine the electrophoresis of a polymer chain through a narrow constriction using a model geometry similar to the entropic trapping device of Han and Craighead (Figure 1). Brownian dynamics simulations are performed to study the electrophoretic motion of a charged bead−rod chain as it moves from one thick channel of the device to the next through the intervening thin channel. Most prior studies on polymer electrophoresis in similar geometries have shown that the transit velocity is determined by the trapping event at the entrance of the thin channel. We find that, in general, the transit velocity is governed by three characteristic time scales associated with (i) the approach of the chain to the entrance of the thin channel as it moves through the first thick channel, τ_{app}, (ii) the trapping or the activation stage at the entrance of the thin channel, τ_{act}, and finally (iii) the passage of the chain through the thin channel, τ_{cross}, ultimately leading to a complete partitioning of the chain in the next thick channel. Each time scale depends on N, with τ_{app} and τ_{act} decreasing with N and τ_{cross} increasing with N. This gives rise to a nonmonotonic dependence of the transit velocity on N, with a maximum occurring at a chain length that represents a transition from a regime where the transport is determined by τ_{act} to one where it is determined by τ_{cross}. The interplay between these two time scales in determining the transit velocity behavior is explored as a function of the applied electric field strength, the size ratio of the thick and thin channels, and channel dimensionality (2D vs 3D). In section 2, we present relevant theoretical background, which is followed in section 3 by a description of the problem setup, polymer model, and simulation method. Results are presented and discussed in sections 4 and 5, with conclusions given in section 6.

2. Theoretical Background

Since the electrophoretic mobility of polyelectrolytes in free solution is independent of chain length,[1,43] size-based separation of DNA is carried out in a sieving matrix such as a gel[44,45] or a microfluidic channel.[2,46] The sieving medium is a network of pores of size ξ connected by narrow constrictions. When $\xi \sim R_g$, the motion of a polymer molecule through the gel is described by the entropic trapping mechanism, which was first proposed by Baumgartner and Muthukumar[47−50] to explain results from simulations of polymers in porous media. They found that polymer chains tend to remain confined within the pores of the matrix since moving out of the pores is associated with a large entropic penalty. Results from later studies on electrophoresis of polymers in porous media were found to be consistent with the idea of entropic trapping.[29,51−53] In addition, experiments that investigated the chain length dependence of polymer mobilities in gels[44,45,54] verified that the motion of the polymer molecules was governed by the entropic trapping effect in the regime where $R_g \sim \xi$.

Microfluidics offers the unique advantage of being able to design a separation medium with controlled pore size distribu-

tion, which can then be used isolate certain dynamical effects (e.g., entropic trapping) for deeper investigation.[55,56] The microfluidic device of Han and Craighead[5] is an entropic trapping device: the thick channels serve as entropic traps whereas the thin channels provide an entropic barrier to the motion of DNA from one trap to the other. The authors have shown that the energy barrier, ΔF_{trap}, associated with the trapping of DNA at the entrance of the thin channel is independent of N and depends only on the electric field present inside the thin channel.[5] The probability of escape was assumed to be proportional to $\exp(\alpha/E_s k_B T)$, where α is a constant, E_s is the electric field strength inside the thin channel, k_B is Boltzmann's constant, and T is the temperature. The authors proposed that the faster escape rate for longer molecules arose from an attempt frequency for barrier crossing which increased with chain length. The attempt frequency is higher for longer molecules because they have more segments facing the entrance of the thin channel, and these attempt to reach a transition state by forming a "hernia" of a critical size inside the thin channel. An expression for the amount of time the molecule spends trapped at the entrance of the thin channel, τ_{trap}, was proposed:

$$\tau_{trap} = \tau_0 \exp(\alpha/E_s k_B T) \quad (1)$$

where τ_0 decreases with N to reflect the attempt frequency. From eq 1, it is clear that a very high value of E_s would lead to a quick escape without trapping while a very low value of E_s would lead to complete trapping of the DNA molecule. Finite trapping times are observed for intermediate values of E_s, where the corresponding $\Delta F_{trap} \sim k_B T$.

Tessier, Labrie, and Slater[30] used a lattice-based Monte Carlo method to simulate the transport of a charged polymer chain in a microchannel based on the Han−Craighead geometry. Results were obtained which showed qualitative agreement with most of the results from Han and Craighead's experiments. Using Monte Carlo simulations with a particle insertion technique, Chen and Escobedo[31] calculated ΔF_{trap} as a function of N at different values of E_s in a geometry very similar to the Han−Craighead device. Their results confirm that τ_{trap} decreases with N when $\Delta F_{trap} \sim k_B T$. Streek et al.[32] used Brownian dynamics simulations to study the electrophoresis of a charged bead−spring chain in the same geometry. They, too, found the mobility to increase with chain length but showed that smaller molecules are also slowed down in their approach to the entrance of the thin channel. They proposed that this slowing down occurs due to diffusion of the smaller molecules to the corners of the thick channel and were able to associate a characteristic time scale with this process.

The translocation of biopolymers through nanopores not only is relevant to understanding physiological phenomena but also inspires design of nanofluidic technologies which promise much faster sequencing methods than current microfluidic-based processes. In addition to experimental studies,[9−15] a number of analytical[16−28] and computational[33−42] studies have examined the problem of driven polymer translocation through a nanopore. Many of these are reviewed in ref 34; here, we focus on the work of Sebastian and Paul[19] because of its relevance to the present study. Sebastian and Paul[19] carried out a detailed analysis of the escape of a polymer molecule over a one-dimensional energy barrier, a biased double-well potential. They considered the motion of the polymer from the metastable well to the other side to be characterized by an activation event and a crossing event. The activation time was found to decrease with N if the polymer reached the activation state in the form of a hairpin-like loop but was found to be independent of N if activation occurred via either of the two chain ends. On the basis of their analysis, a general expression for the activation time, τ_{act}, would look like

$$\tau_{act} = \tau_p \exp(\Delta F_{act}/k_B T) \quad (2)$$

where ΔF_{act} is the free energy barrier (which depends only on the magnitude of the applied potential gradient) and τ_p (which depends on the magnitude of the applied potential gradient and N) is a prefactor characterizing the attempt frequency. It was shown that $\Delta F_{act,hp}$ (hairpin) $= 2\Delta F_{act,end}$ (end) because a looped chain can be considered as two chains crossing end-first. The prefactor $\tau_{p,hp}$ was shown to scale as N^{-1} because a chain offers N sites for hairpin formation, while $\tau_{p,end}$ was independent of N since all linear chains have only two ends. The activation event is followed by a downhill crossing event, where the chain has to slide over the barrier in order to lie completely on the stable side of the double well. The crossing time, τ_{cross}, associated with this process was shown to increase linearly with N.

Sebastian and Paul argued that in the Han−Craighead device activation by hairpin formation would be greatly favored over end-activation as N becomes large. Then, $\tau_{act,hp}$ would determine the trapping time for a polymer molecule, which is consistent with the results of Han and Craighead[5] where the trapping time was found to decrease with N. They further claimed that in the nanopore experiments of Kasianowicz et al.[9] the small diameter of the pore permits the polymer chain to enter only by one of its ends, which results in an activation event independent of N. In this case, the translocation time is determined by τ_{cross}, which increases linearly with N and thus explains why the blockade times in the nanopore experiments were found to increase with N. Although Sebastian and Paul show how a specific time scale can determine the transit velocity in a particular experiment, they do not consider the case where more than one time scale could influence the transit velocity of the polymer. In our study, we show how the interplay between the different time scales associated with the transit of the polymer through a narrow constriction leads to a nonmonotonic dependence of the transit velocity on the chain length.

3. Description of Model and Simulations

3.1. Problem Setup and Polymer Model. Figure 1 shows a schematic of the model entropic trapping geometry used in this study. The length L_c represents the pitch length of the model geometry, which is repeated in the x-direction to obtain a series of entropic traps separated by entropic barriers. For the majority of the simulations, the channel is assumed to extend infinitely in the z-direction, but we have also considered 2D channels where the polymer is confined to the $x-y$ plane. The heights of the thick and thin channels are h_l and h_s, respectively, and they are both assumed to be of equal length $L_c/2$. An electrostatic potential drop of ΔV_{app} is applied across the length L_c. The potential inside the channel, $V_c(x,y)$, is calculated by solving the 2D Laplace equation using a finite-difference scheme which yields values of V_c on a grid of size a. We assume that the walls of the channel are insulating and that the solution obtained is periodic in the x-direction. When the Brownian dynamics simulations are carried out, the potential at arbitrary points inside the channel is obtained by interpolating between those evaluated at the grid points. Biquadratic basis functions are used for interpolation, which ensure continuity of the electric field, $\mathbf{E}_c$, computed inside the channel. Similar approaches have been used in other molecular simulations.[30−32] This way of calculating the electric field assumes that the charged polymer does not have any effect on the electric field inside the channel.

The polymer is modeled as a freely jointed bead−rod chain of N beads connected by $N - 1$ rigid rods, where the length of each rod corresponds to a Kuhn step, denoted by b_K. The total charge along the backbone is distributed uniformly among all the beads by assigning each bead a charge q, but the beads are not allowed to interact electrostatically with one another. We also note that excluded-volume interactions are not included in the description of the polymer, which implies that we are simulating "phantom chains". However, Kantor and Kardar[42] have shown in their study on forced polymer translocation that excluded-volume effects could affect translocation dynamics. Each bead in the chain represents a Brownian particle whose motion is governed by an inertialess Langevin equation, which describes the balance of forces acting on the bead. This can be rewritten as a stochastic differential equation describing the evolution of the position of the ith bead, $\mathbf{r}_i$, with respect to time, t:

$$\zeta \frac{d\mathbf{r}_i}{dt} = \mathbf{F}_i^B + \mathbf{F}_i^T + \mathbf{F}_i^P + \mathbf{F}_i^E \tag{3}$$

which is integrated to obtain new bead positions after every time step. Here, ζ is a scalar drag coefficient associated with every bead, $\mathbf{F}_i^B$ is the random Brownian force exerted by the solvent molecules, $\mathbf{F}_i^T$ is the constraint force on bead i due to the two rods connected to the bead, $\mathbf{F}_i^P$ is a pseudopotential force added to obtain the correct probability distribution for the bead−rod chain, and $\mathbf{F}_i^E$ is the external force acting on each bead due to the externally applied electric field. Details about the terms in eq 3 have been described by us elsewhere.[57] However, there are two comments worth mentioning here. First, we have used Grassia and Hinch's[58] method for calculating the pseudopotential forces, which enables us to carry out the procedure in $O(N)$ steps. Second, as have prior studies,[30−32] we have neglected hydrodynamic interactions (HI). In the case of free-solution electrophoresis, HI are screened because the flow of counterions exactly cancels the hydrodynamic flow induced by the motion of the polymer segments. It has been shown that HI become important if tension builds up along the chain,[59] which could arise if the chain encounters an obstacle. In their Monte Carlo simulations, Tessier et al.[30] point out that HI are most likely present in the actual scenario but not considering them does not qualitatively change the basic trapping behavior.

In our simulations, all lengths are scaled by the Kuhn length, b_K, times by a relaxation time, $\zeta b_K^2/k_BT$, and forces by k_BT/b_K. The expression for the nondimensional external force is given by

$$\mathbf{F}_i^E = \frac{qe\mathbf{E}_c}{k_BT/b_K} \tag{4}$$

where q is the charge on each bead and e is the electron charge.

3.2. Simulation Algorithm and Parameters. Equation 3 is integrated using the mid-step algorithm developed by Grassia and Hinch.[58] Details of the algorithm can be found in the papers by Fixman,[60] Hinch,[58] and Morse.[61] This algorithm involves a truncation error which causes the link lengths to deviate from their prescribed value. To maintain their inextensibility, link lengths are checked at the end of every time step. If a link is found to deviate by more than 0.05%, it is regrown to the prescribed value while maintaining its orientation. As the chain moves through the channel, beads can be found to lie outside the channel when the chain is in the vicinity of the channel walls. Such a situation could arise, for example, when the chain is either trapped at the entrance of the narrow constriction or as it moves through the narrow constriction. The polymer is confined inside the channel by imposing Monte Carlo-like boundary conditions, where Brownian dynamics moves which result in any bead lying outside the channel are rejected. In such a case, the beads are assigned their original positions, and forces are recalculated to give new positions which are again checked for boundary violations.

Polymer properties are calculated as averages over an ensemble of 100 chains, which was found sufficient to obtain convergence in the properties we calculated. Initial configurations corresponding to a Gaussian distribution of the end-to-end distance are generated before starting the simulations. The center-of-mass of each configuration is placed at the point (0, 10, 0) at the start of the simulation. The simulation is stopped when the entire chain exits the thin region, i.e., when the bead with the smallest x-coordinate finds itself out of the thin region.

The grid size used in the finite difference scheme is $a = 0.2b_K$, the pitch length of the channel is fixed at $L_c = 80$, and chains of sizes $N = 50$, 100, 200, and 300 are considered. We assume a dimensional value of $b_K = 50$ nm, which is comparable to persistence length values observed for DNA (30−60 nm).[1] The average scalar electric field strength, defined as $E_{av} = \Delta V_{app}/L_c$, is varied between dimensionless values of 0.056 and 0.355. These values of E_{av} correspond to dimensional values of 2−12.5 V/cm, which are smaller than those used in the Han−Craighead experiments, where entropic trapping effects were observed for electric field values between 30 and 60 V/cm. The differences in the experimental and simulation values of E_{av} may be due to effects not included in the simulations such as excluded volume, electrostatic, and hydrodynamic interactions, uncertainty in the some of the parameter values used to calculate $\mathbf{F}_i^E$ (we took a base-pair length of 0.34 nm and a base-pair charge of unity with $T = 300$ K), and differences in the chain lengths considered (the chains in the simulations are shorter than those in the experiments). The height of the thick channel is fixed at $h_l = 20$, and only the value of h_s is varied in order to study the effect of the relative size of the thick and thin channels. This value of h_l is comparable to R_g for the chain lengths considered here and is equal to 1 μm in dimensional units, while the pitch length is $L_c = 4$ μm in dimensional units. Both of these values compare well with values from Han and Craighead's experiments.

4. Results and Discussion: Description of Characteristic Times

We first present results for the case where $E_{av} = 0.071$ and $h_s = h_l/10 = 2$. The particular value of $h_s = 2$ was chosen because it corresponds to a dimensional value of 100 nm, which is similar to the height of the thin channel in the experiments of Han and Craighead. For a value of $E_{av} = 0.071$, polymer chains were found to be entropically trapped inside the thick channel and displayed trapping times which decreased with N. Choosing this value of E_{av} also ensured that the simulations could be carried out in a reasonable amount of time. In section 5, where we conduct a parametric study, we will use this case as a reference to make comparisons.

We now describe the definitions we have used for τ_{app}, τ_{act}, and τ_{cross} in our study. Parts a−c of Figure 2 each show two instants in time, the one on the left marking the onset of an event and the one on the right the completion of the event. The solid arrows indicate progress in time and represent time intervals corresponding to the (a) approach, (b) activation, and (c) crossing events. Since net motion occurs in the x-direction,

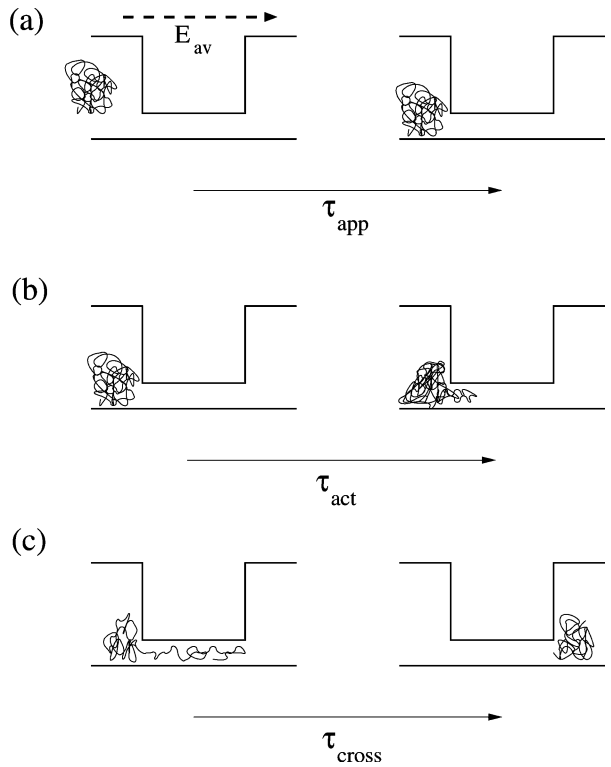

Figure 2. Schematics which depict the three consecutive events involved in the transit of the polymer through the narrow constriction: (a) approach, (b) activation, and (c) crossing.

we use the *x*-coordinate of the bead which leads all other beads in the chain, x_{lead}, and that of the bead which lags behind all others, x_{lag}, to define events. Thus, from Figure 2a, τ_{app} corresponds to the time it takes for x_{lead} to reach a value of 19.5 (in close proximity to the trap) starting from its initial position where the center of mass is situated at (0, 10, 0). According to Figure 2b, τ_{act} corresponds to the time it takes for x_{lead} to move from a value of 19.5 to $x_{lead} = x_c$, where x_c corresponds to the location of the top of the activation energy barrier. As shown in the schematic, this activation is achieved by a small part of the chain finding its way into the thin channel. Following this event, the crossing event takes place (Figure 2c), and τ_{cross} is defined as the time between the instants when $x_{lead} = 60$ and when the entire chain finds itself in the next thick channel, corresponding to $x_{lag} = 60$. Between the activation and crossing events defined above, a finite amount of time elapses between the instants when $x_{lead} = x_c$ and $x_{lead} = 60$. However, this time slab was found to be independent of *N* and will not be considered here as a relevant time scale. This event corresponds to a train of beads moving over a distance of $60 - x_c$, which would be independent of *N* for chains longer than the length of the thin channel ($N > 40$).

In Figure 3a−d, we show how the different time scales discussed above and the transit velocity of the chain, $v_{transit}$, vary with *N*. While Figure 3a,b shows τ_{app}, τ_{act}, and τ_{cross}, Figure 3c plots the total transit time, $\tau_{transit}$, required for the polymer to completely move out of the thin channel. Here, $\tau_{transit}$ is defined as a sum of the other three times:

$$\tau_{transit} = \tau_{app} + \tau_{act} + \tau_{cross} \tag{5}$$

Thus, the definition of $\tau_{transit}$ does not include the *N*-independent time slab discussed at the end of the last paragraph but has contributions only from *N*-dependent time scales. However,

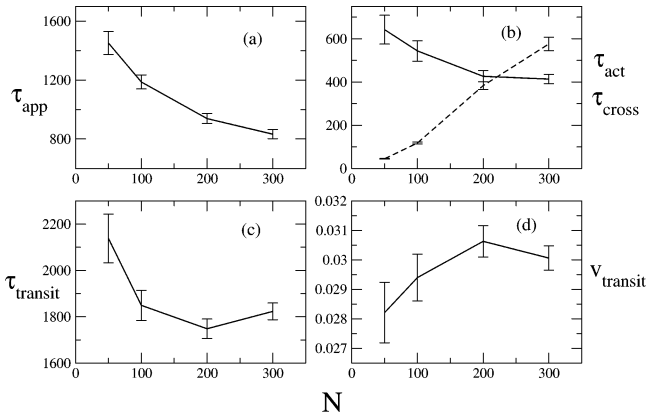

Figure 3. Different time scales shown as functions of *N* for the case of $E_{av} = 0.071$, characterizing (a) approach, (b) activation (solid line) and crossing (dashed line), and (c) total transit. Panel (d) shows the transit velocity as a function of *N*.

$v_{transit}$ (Figure 3d) does include this time slab since it is defined as

$$v_{transit} = \frac{x_{lead,f} - x_{lead,i}}{t_{sim}} \tag{6}$$

where $x_{lead,f}$ and $x_{lead,i}$ are the values of x_{lead} at the end and the beginning of the simulation, respectively, and t_{sim} is the time taken to move between these two values of x_{lead}. The error bars in Figure 3 and in all other plots presented here represent the standard deviation within the ensemble of chains considered. With respect to size-based separation of polymers by electrophoresis, these error bars can be related to the resolution of separation. If the error bars in time or velocity corresponding to two different chain sizes show a considerable overlap, it implies that the two size fractions move with similar speeds. We now discuss each of these figures in detail.

Approach Time. We find that τ_{app} decreases nonlinearly with *N* (Figure 3a), which indicates that shorter chains take more time to travel to the entrance of the thin channel. Streek et al.[32] have suggested that in the entropic trapping device smaller molecules are slowed down due to diffusion to areas in the thick channel where the strength of the electric field is weak. Since entropic trapping is observed for weak electric fields ($\Delta F \sim k_B T$), thermal diffusion can significantly affect transport in the thick channel and can lead a chain into a region where the electric field is not strong enough to drive the chain to the entrance of the thin channel. Streek et al. have shown that small chains can remain trapped in such regions over time scales which are longer than the trapping time scales. They also found that the probability of such a trapping event taking place decreases with both chain length and the strength of the applied electric field. Our results for approach times are in line with these observations. A shorter τ_{app} for a longer chain could also result from its larger size (R_g) because parts of a longer chain may lie simultaneously in areas of weak and strong electric field. Thus, parts of the chain which lie in areas of strong electric field are driven toward the entrance of the thin channel, which results in the entire chain moving there. Another consequence of a larger size arises from the initial condition, where all chains start with their centers-of-mass at (0, 10, 0), so a larger chain is closer to the entrance of the thin channel to start with when compared to a smaller chain.

Activation Time. To calculate τ_{act}, we first need to know the critical distance, x_c, inside the thin channel which the chain needs to penetrate in order to reach the transition state. Tessier

et al.[30] calculated x_c by plotting the distribution of x_{lead} as a function of distance along the channel and then fitting the portion inside the thin channel to a function $\rho(x_{lead}) = \rho_0 \exp(-x_{lead}/x_c)$, where the decay length x_c corresponds to the critical distance. Following their example, we calculated x_c for different values of N and found x_c to depend only on E_{av}. With this information, we then calculated activation times for different chain lengths (Figure 3b). We found that τ_{act} decreases with N, consistent with the experimental observations of Han and Craighead[5] and the results from previous simulation studies.[30−32] From their analysis, Sebastian and Paul[19] had shown that if escape over the energy barrier occurred by the formation of a hairpin-like loop, then the rate of escape over the barrier would increase with N. This would happen because the probability of forming such a loop increases with N, and in such a case, τ_{act} would decrease with N. Since we observe a decrease in τ_{act} with N, our results suggest that escape into the thin channel takes place in this way. Han and Craighead have argued that longer chains escape faster because they have more segments facing the entrance of the thin channel.[5] This idea is equivalent to the idea of Sebastian and Paul since a larger number of segments facing the channel entrance implies that there are more segments present which can form a loop. However, it is not immediately clear whether a loop would form in the $x-y$ plane or the $y-z$ plane; the spreading of the chain along the z-direction could influence the dependence of τ_{act} on N. We discuss this issue in section 5.

Crossing Time. Unlike τ_{app} and τ_{act}, τ_{cross} is found to increase with N (Figure 3b). Since crossing is defined as the transit of N segments of the chain through the thin channel, we expect τ_{cross} to increase with N. Upon fitting the crossing time data to a power law, we find that $\tau_{cross} \sim N$, which is consistent with Sebastian and Paul's analysis. Our results are also in line with the experimental results of Kasianowicz et al.,[9] where the blockade times were found to increase linearly with N.

Transit Time and Transit Velocity. From Figure 3c, we find that $\tau_{transit}$ depends nonmonotonically on N. It first decreases with N, reaches a minimum around $N = 200$, and then increases with N. As a consequence, $v_{transit}$ first increases with N, reaches a maximum, and then drops with further increase in N (Figure 3d). It is immediately apparent from Figure 3c,d that the values of N at which the corresponding minimum and maximum occur for $\tau_{transit}$ and $v_{transit}$ are the same. This also supports the argument that the time slab between activation and crossing is independent of chain length and can be safely ignored in the analysis.

This behavior of $v_{transit}$ is in contrast to what is observed in the entropic trapping experiment where $v_{transit}$ increases with N (ref 5) or the nanopore translocation experiment where $v_{transit}$ decreases with N (ref 9). The reason for the nonmonotonic dependence of $v_{transit}$ on N is that the three time scales not only contribute numerically to $\tau_{transit}$ but also determine the functional dependence of $v_{transit}$ on N. From Figure 3b, we find that at $N = 200$, τ_{act} and τ_{cross} become comparable to each other. Below this crossover value, $\tau_{act} > \tau_{cross}$, and $v_{transit}$ increases with N. Here, smaller chains are slowed down in comparison to longer ones, because of both their slower approach and their longer activation times at the barrier. Above this value of N, $\tau_{act} < \tau_{cross}$, and the crossing event dominates the transport of the chain in the model geometry. Moving into the second thick channel becomes more difficult with increasing N since more segments now have to move across the thin channel, leading to a decrease in $v_{transit}$ with N. Therefore, the crossover value of N denotes a transition value below which the activation event determines the motion of the chain and above which the motion is determined by the crossing event. Such a transition between these two processes demonstrates that there could exist conditions in polymer electrophoresis through narrow constrictions under which more than one physical mechanism could determine the behavior of the transit velocity. A nonmonotonic dependence of DNA electrophoretic mobility on chain length has also been reported by Streek and co-workers[62] in a study where they investigated DNA migration in a topologically structured microchannel. However, in their study both the geometry of the microchannel and the origin of the nonmonotonic behavior are different from what is described here. They considered microchannels which are characterized by $h_l = 2h_s$ and $h_s \sim R_g$. In addition, the nonmonotonic behavior arises from the DNA migrating between fast and slow moving states inside the microchannel at high electric field strengths. In the following section, we discuss how E_{av} and the geometry of our model entropic trapping device affect the nature of the transit velocity and characteristic time curves.

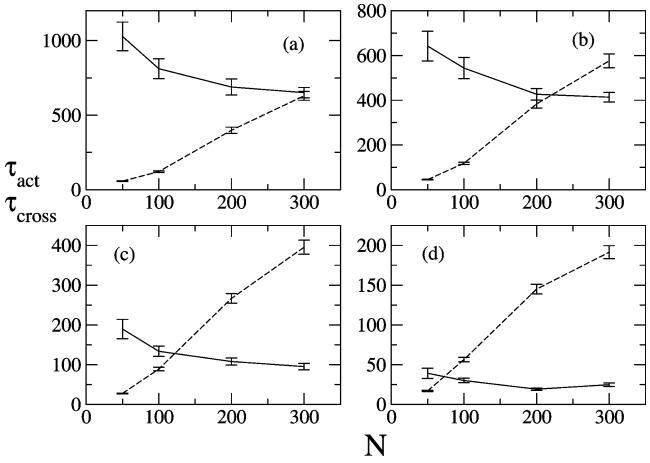

Figure 4. Crossover of τ_{act} (solid lines) and τ_{cross} (dashed lines) shown at different values of E_{av}: (a) $E_{av} = 0.056$, (b) $E_{av} = 0.071$, (c) $E_{av} = 0.142$, and (d) $E_{av} = 0.355$.

5. Results and Discussion: Parametric Study

5.1. Effect of Field Strength. In Figure 4 we show τ_{act} and τ_{cross} for four different values of E_{av}: (a) $E_{av} = 0.056$, (b) $E_{av} = 0.071$, (c) $E_{av} = 0.142$, and (d) $E_{av} = 0.355$. Figure 4b corresponds to the reference case considered in the previous section. We find that both τ_{act} and τ_{cross} decrease for all values of N as E_{av} is increased, which is consistent with our expectation that faster motion will occur in the presence of a stronger driving force. On the basis of the analysis of Sebastian and Paul,[19] we can write the electric field dependences of τ_{act} and τ_{cross} in the following manner:

$$\tau_{act} \sim \frac{1}{N\sqrt{E_{av}}} \exp\left(\frac{\epsilon}{E_{av}}\right)$$

$$\tau_{cross} \sim \frac{N}{\sqrt{E_{av}}} \qquad (7)$$

where ϵ is a constant. Then, a crossover between these two times occurs when $\tau_{act} = \tau_{cross}$, corresponding to a crossover chain length, N_{cr}, which is proportional to $\exp(\epsilon/2E_{av})$. This implies that N_{cr} decreases as E_{av} increases, and the behavior observed in Figure 4 reflects this argument. The crossover is observed at $N > 300$ for $E_{av} = 0.056$, but as E_{av} increases N_{cr} falls to around 220 for $E_{av} = 0.071$, about 120 for $E_{av} = 0.142$, and close to 75 for the highest electric field strength studied here, $E_{av} =$

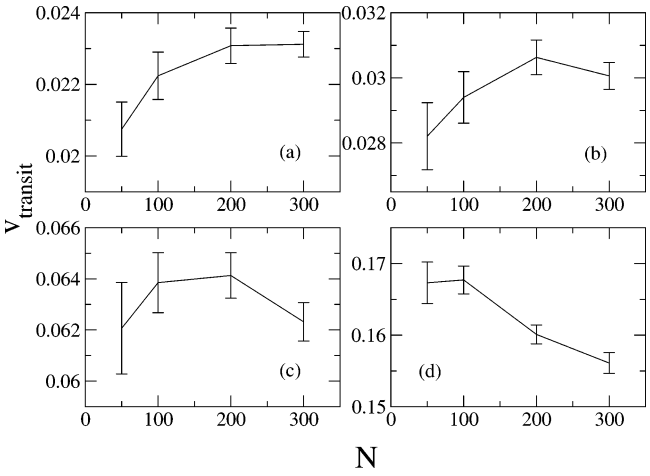

Figure 5. The quantity $v_{transit}$ shown as a function of N at different values of E_{av}: (a) $E_{av} = 0.056$, (b) $E_{av} = 0.071$, (c) $E_{av} = 0.142$, and (d) $E_{av} = 0.355$.

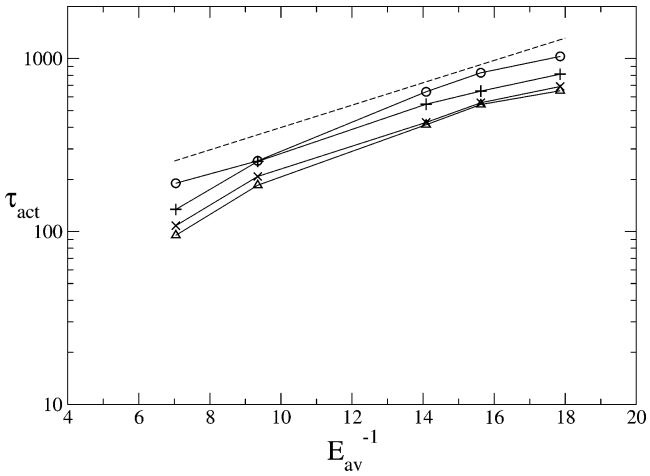

Figure 6. The quantity τ_{act} plotted as a function of $1/E_{av}$ on a semilog scale. The different series in the plot correspond to different values of N: $N = 50$ (○), $N = 100$ (+), $N = 200$ (×), and $N = 300$ (△). The dashed line is a fit to the data for $N = 50$, and the solid lines serve as guides to the eye.

0.355. In accordance with the results from the previous section, we find that for all four cases N_{cr} also corresponds to the value of N at which a maximum is observed in $v_{transit}$, as seen in Figure 5. For $E_{av} = 0.056$ (Figure 5a), we find that $v_{transit}$ increases with N but seems to be approaching a maximum around $N = 300$ as is evident from the decreasing slope of the curve. The expected position of the maximum (at $N > 300$) agrees well with the expected crossover value of N in Figure 4a. Similar agreement between the maxima in $v_{transit}$ (Figure 5b−d) and the occurrences of N_{cr} (Figure 4b−d) is also observed for all other values of E_{av}.

The shifting of N_{cr} to smaller values with increasing E_{av} implies that the transition from an activation-dominated regime to a crossing-dominated regime occurs much earlier as E_{av} increases. At $E_{av} = 0.056$, $N_{cr} > 300$, and one would expect N_{cr} to increase even more if E_{av} falls below 0.056. This means that at low enough values of E_{av}, N_{cr} could shift to much larger values of N such that $\tau_{act} > \tau_{cross}$ for all relevant chain lengths ($h_l \sim R_g$). In such a situation, one would observe that $v_{transit}$ increases with N as both τ_{app} and τ_{act} decrease with N. Since $\tau_{cross} < \tau_{act}$ for all relevant values of N, the crossing event would not have any effect on behavior of $v_{transit}$. Such a picture helps us better understand the results from the entropic trapping experiment, where in the presence of low electric fields τ_{act} appears to be the only relevant time scale. In the other extreme, if E_{av} increases to a higher value for which N_{cr} shifts to very small values of N, then one would expect $v_{transit}$ to be dominated by the crossing event. For the case of $E_{av} = 0.355$, we find that $v_{transit}$ decreases with N for the most part, except in a very small region between $N = 50$ and $N = 100$ where the velocity is nearly constant (Figure 5d). By examining the plots of τ_{act} and τ_{cross}, we find that N_{cr} is very small, and there exists a large region where $\tau_{cross} > \tau_{act}$. We can anticipate that as E_{av} increases, the height of the entropic barrier falls down and causes activation to become an insignificant part of the process. This would lead to a situation where $\tau_{cross} > \tau_{act}$ for all chain lengths, and as a consequence, longer chains would have a smaller transit velocity than shorter chains. In fact, the mobility data for T2 (longer) and T7 (shorter) DNA from Han and Craighead's experiments[5] show that above $E_{av} = 60$ V/cm, T7 DNA has a higher mobility than T2 DNA. In the experiments, this value of the field also corresponds to the end of the entropic trapping regime.

We now discuss the electric field dependence of τ_{app}, τ_{act}, and τ_{cross}. In Figure 6, τ_{act} is plotted as a function of $1/E_{av}$ for different values of N. The curves show that at a given E_{av}, τ_{act} decreases with N, and for a given N, it increases with E_{av}. On the semilog scale shown here, all four curves are nearly parallel to each other, and τ_{act} is found to vary linearly with $1/E_{av}$. This implies that the activation energy barrier depends only on E_{av} and that $\tau_{act} \sim \exp(\epsilon/E_{av})$. Tessier et al.[30] and Chen and Escobedo[31] have also reported this dependence of τ_{act} on E_{av} in their simulation studies. This implies that our simulation results capture the electric field dependence of τ_{act} on E_{av} as was described by the simple scaling relationship proposed by Han and Craighead.[5]

We know from eq 7 that $\tau_{cross} \sim N/\sqrt{E_{av}}$. Indeed, it was found that for $\tau_{cross}\sqrt{E_{av}}$ plotted as a function of N, all the data corresponding to different values of E_{av} collapsed onto a single curve, which is consistent with the scaling result of eq 7. For the approach time data, $\tau_{app}E_{av}$ was plotted as a function of N, and in this case, too, all curves collapsed onto a single curve. This suggests that τ_{app} is inversely proportional to the applied electric field strength, E_{av}, which is consistent with the results of Streek et al.[32]

5.2. Effect of Height Ratio. To assess the effect of the ratio h_s/h_l on chain transport, simulations were carried out for $h_s = 2$, 4, 6, and 20, corresponding to $h_s/h_l = 0.1$, 0.2, 0.3, and 1. In Figure 7, we have plotted the x-component of the electric field, E_x, as a function of distance along the channel for the different values of h_s considered here. As shown in the schematic of the channel within the plot, E_x values are recorded along the plane $y = h_s/2$ (dotted line). We find that as h_s increases, the value of E_x increases in the thick channels but decreases in the thin channel. The horizontal line at $E_x = 0.071$ corresponds to the case where the channel is of uniform thickness h_l, which results in an electric field that is one-dimensional and uniform everywhere.

In Figure 8, we plot the characteristic times for $h_s = 2$ and $h_s = 6$. From Figure 8a, we find that τ_{app} decreases for all values of N when h_s is increased from 2 to 6. Since the value of E_x in the thick channel is higher for $h_s = 6$ (Figure 7), this leads to a decrease in τ_{app} when h_s is increased. We find that τ_{act} decreases for all values of N when h_s is increased from 2 to 6 (Figure 8b). When the height of the thin channel is increased, a polymer chain which attempts to enter this region pays a smaller entropic penalty because it has more room to move about. This reduces the activation energy barrier at the entrance of the thin channel, leading to a decrease in τ_{act}. The values of

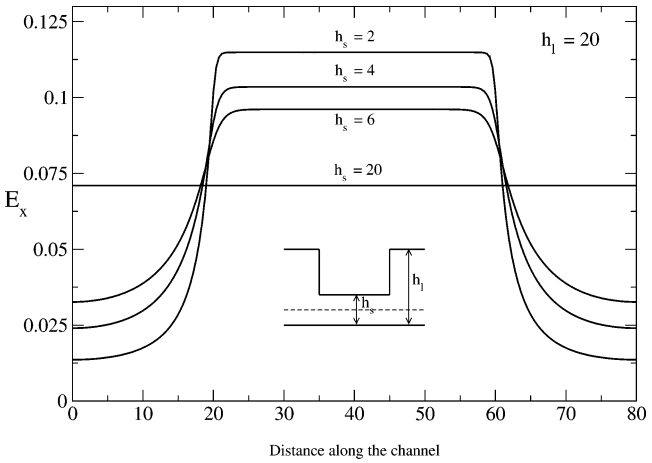

Figure 7. The *x*-component of the electric field inside the channel, E_x, measured along the plane $y = h_s/2$, and plotted as a function of distance along the length of the channel for different values of h_s, and a fixed value of $h_l = 20$. The average value of the electric field in all cases is $E_{av} = 0.071$.

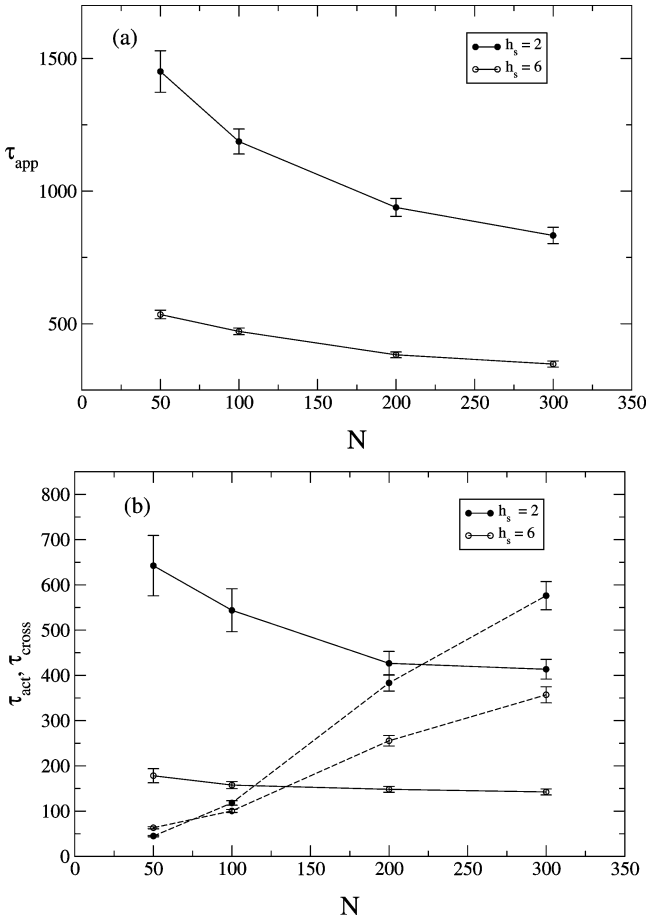

Figure 8. (a) Approach time, τ_{app}, plotted as a function of N and (b) crossover of τ_{act} (solid line) and τ_{cross} (dashed line), shown for the two cases of $h_s = 2$ and $h_s = 6$.

τ_{cross} also decrease for most values of N as h_s increases from 2 to 6. It is only in a small region below $N \approx 75$ where the values of τ_{cross} corresponding to $h_s = 2$ are smaller than those corresponding to $h_s = 6$ (Figure 8b). An increase in h_s also implies that more beads of the chain can be present at a given *x*-position along the thin channel, which results in more segments crossing into the next thick channel at the same time and a decrease in the value of τ_{cross} for most N. Even though the value of E_x in the thin channel decreases with increasing

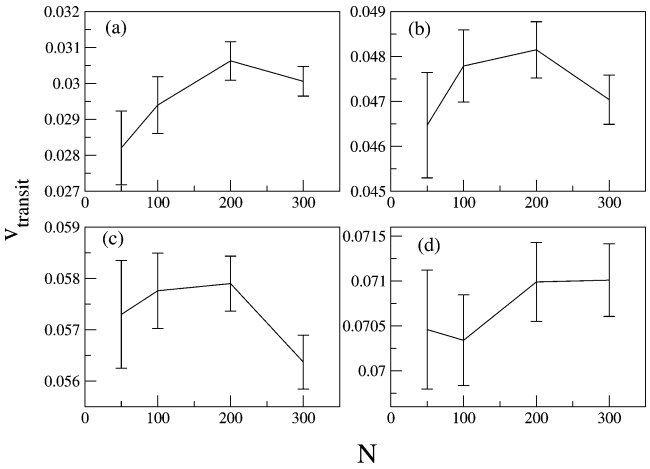

Figure 9. The quantity $v_{transit}$ shown as a function of N at different values of h_s: (a) $h_s = 2$, (b) $h_s = 4$, (c) $h_s = 6$, and (d) $h_s = 20$.

h_s, it does not lead to an increase in either τ_{act} or τ_{cross} as one might expect from eq 7.

A decrease in the values of τ_{act} and τ_{cross} leads to a shift in N_{cr} to smaller values and also reduces the separation between τ_{act} and τ_{cross} for $N < 200$. The consequences are apparent in Figure 9, where $v_{transit}$ is plotted as a function of N for (a) $h_s = 2$, (b) $h_s = 4$, (c) $h_s = 6$, and (d) $h_s = 20$. As h_s increases from 2 to 20, $v_{transit}$ increases as a result of a decrease in all characteristic times. Since N_{cr} shifts to smaller values as h_s increases, we expect the occurrence of the maximum in $v_{transit}$ to shift to smaller values of N_{cr} on the basis of the results from section 5.1 (Figures 4 and 5). In Figure 9a−c, the shift in the maximum to smaller values of N is not immediately clear, and the maximum value of $v_{transit}$ seems to remain at around $N = 200$. However, visual inspection suggests that the slope of the $v_{transit}$ curve near the maximum decreases as h_s increases from 2 to 6. We also find that as h_s increases, the difference in $v_{transit}$ begins to diminish between chains of different lengths. In Figure 9c ($h_s = 6$), we find that $v_{transit}$ does not change much for $N = 50$, 100, and 200 and then decreases for $N = 300$. This behavior is consistent with the reduced separation observed between τ_{act} and τ_{cross} for $h_s = 6$ (Figure 8b). Figure 9d corresponds to the case where the channel has a uniform thickness and uniform electric field strength. Although we do not observe any systematic trends in the data for this case, we note that there is a considerable overlap in the error bars corresponding to all values of N. In the case of free-solution electrophoresis, one would obtain uniform velocities for all values of N (ref 34). Since Figure 9d corresponds to a channel with a finite thickness, it is possible that interaction of the polymer chain with the channel walls leads to slight differences in $v_{transit}$ for different values of N.

5.3. Effect of Dimensionality. We studied the effect of the depth of the geometry in the *z*-direction on the transport of the chain by carrying out 2D simulations which confined the chain to the *x*−*y* plane of the channel. Here, we compare results from the 2D and 3D simulations for the case where $E_{av} = 0.071$; $h_l = 20$ and $h_s = 2$ in both situations. In Figure 10a, we plot τ_{act} and τ_{cross} for the two cases. Even in a 2D channel, τ_{act} is found to decrease with N. Han and Craighead[5] proposed that faster activation occurs for longer chains because they have more monomers in contact with the interface of the thick and thin channels. This idea suggests that longer chains have a higher probability of nucleating loops which venture into the thin channel because of their greater size in the *y*−*z* plane. This picture would not be valid for the case of a 2D channel where

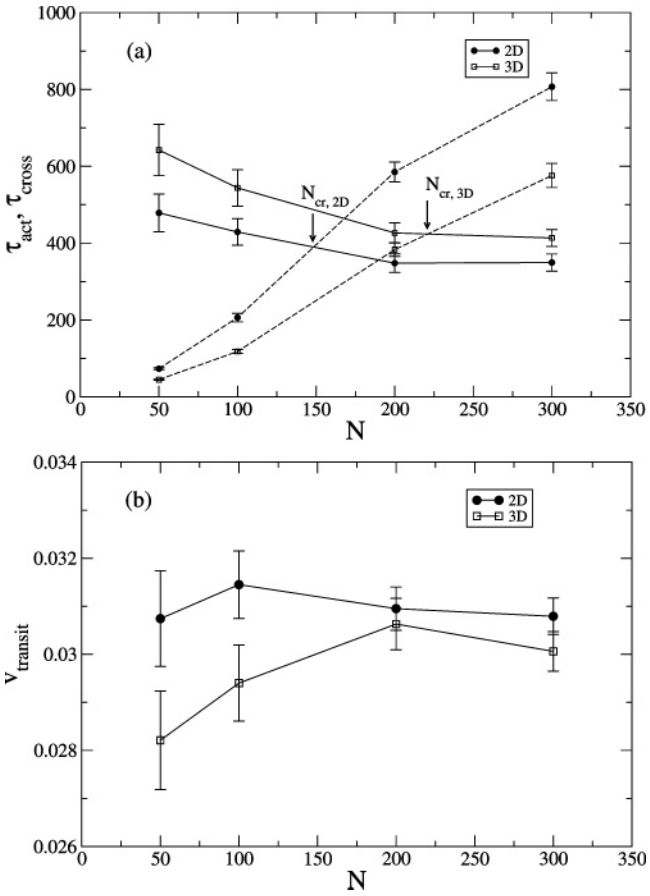

Figure 10. (a) Crossover of τ_{act} (solid line) and τ_{cross} (dashed line) and (b) $v_{transit}$ as a function of N, for the two cases of a 2D channel and 3D channel.

all chains (with $R_g \sim h_l$) would present almost the same number of monomers at the entrance of the thin channel. In contrast with the 3D channel, where a loop can form such that it has a projection in the $x-z$ plane, a loop can form only in the $x-y$ plane in a 2D channel. Hence, a decrease in τ_{act} with N for the 2D channel implies that the probability of loop formation indeed increases with N, as has been previously predicted by Sebastian and Paul.[19] However, this does not mean that the lateral extent of the chain in the 3D channel does not influence the trapping behavior. Tessier et al.[30] have shown in their simulations that the chain adopts the shape of an ellipsoidal pancake at the entrance of the thin channel prior to reaching the transition state. The chain was shown to deform in the z-direction, characterized by an increase in the z-component of the radius of gyration, and a greater deformation was observed for longer chains and at lower electric fields. They pointed out that a deformation in the z-direction could influence the trapping behavior at low electric fields, when such processes could occur faster than the activation time of the chain. A larger size of the chain in the z-direction could possibly lead to several escape loops forming simultaneously, a scenario which would become less likely as one increases E_{av}.

From Figure 10a, we observe that activation times are larger in the 3D channel than in the 2D channel. The presence of an additional dimension may allow the chain to spend time relaxing in the z-direction upon reaching the entrance of the thin channel, thereby prolonging the activation process. The effect of dimensionality on the crossing times is the reverse of that for the activation times. Although τ_{cross} increases with N for the 2D channel, the values for any N are higher when compared to the 3D channel. In a 3D channel, more than one segment can be present at the same x-coordinate because the chain can spread in the z-direction. As a result, more than one segment can move out of the narrow constriction at the same time, leading to faster crossing rates in the 3D channel. (More than one bead can be present at the same x-coordinate in the narrow constriction of a 2D channel. But the likelihood of this happening is expected to be smaller than in a 3D channel since the narrow constriction is only two Kuhn steps wide.) Thus, a lowering of τ_{act} and an increase in τ_{cross} for the 2D channel shifts N_{cr} to smaller values ($N_{cr,2D} \approx 150$ and $N_{cr,3D} \approx 220$). Consequently, the maximum in $v_{transit}$ also shifts to smaller values of N for the 2D channel (Figure 10b). In addition, the chain moves faster in the 2D channel. For smaller N, where transport is determined by the activation event, and τ_{act} is larger for the 3D channel, the difference in $v_{transit}$ for the two cases is large. As one moves to larger N and transport begins to be determined by the crossing event, the difference in $v_{transit}$ for the two cases becomes smaller since τ_{cross} is smaller for the 3D case. One might then speculate that for a situation dominated by the crossing event velocities may be higher in the 3D channel.

To test this conjecture, we carried out simulations where the initial condition corresponds to a conformation where one end of the chain is placed at (19.9, 1, 0), which is a point very close to the entrance of the thin channel. With this initial condition, we expect that the probability of end-activation would be enhanced, and most chains would enter the thin region end-first. These simulations were carried out for both the 2D and 3D channels for $E_{av} = 0.071$. The results are summarized in Figure 11, where we note two important observations. First, we find that τ_{act} is independent of N for both the 2D and 3D channels. This is consistent with the prediction of Sebastian and Paul[19] that the end-activation rate for a polymer is independent of chain length. The other observation is that τ_{cross} is higher for the 2D channel, which agrees with results from Figure 10. Consequently, we find that $v_{transit}$ decreases with N (Figure 11b) since the chain length dependence of the polymer speed arises only out of the crossing event and that $v_{transit}$ is higher for the 3D channel. This is in line with the speculation raised at the end of the previous paragraph.

These observations may also provide some insight into the mechanism of polymer translocation through a nanopore. In that case, the size of the nanopore is so small that the polymer can enter the pore only by one of its ends. Then, as predicted by Sebastian and Paul, τ_{act} should be independent of N and τ_{cross} should increase with N, and as a result, $v_{transit}$ should decrease with N. Our simulations with end-activated transit for the cases of both the 2D and 3D channels seem to support this picture and are consistent with the findings of Kasianowicz et al.,[9] where $v_{transit}$ was found to decrease with N. However, if the size (diameter) of the nanopore is increased one may begin to observe both end-activated and hairpin-activated transit. More recent experiments[11−15] on translocation of double-stranded DNA through nanopores larger (8−10 nm) than those used by Kasianowicz et al.[9] have demonstrated that the DNA can enter the nanopore either by forming a loop or in a linear fashion using one of its ends.

6. Conclusions

Using Brownian dynamics simulations, we have studied the electrophoresis of a charged bead−rod chain through a narrow constriction which is a thin channel that separates two thick channels. The transit of the polymer chain from one thick channel of the device to the other can be characterized by three

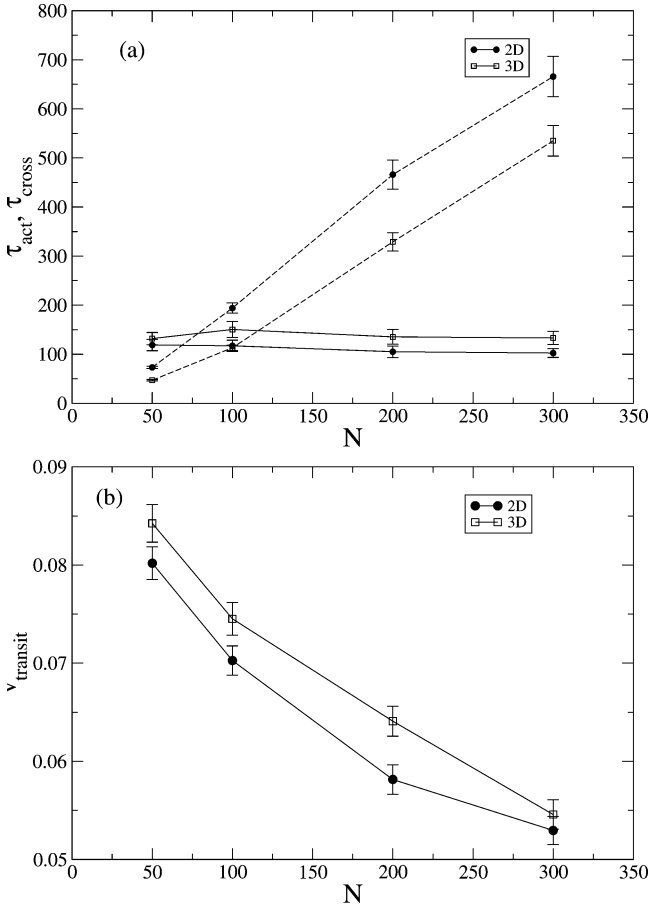

Figure 11. (a) Crossover of τ_{act} (solid line) and τ_{cross} (dashed line) and (b) $v_{transit}$ as a function of N, for the two cases of a 2D channel and 3D channel when an end of the chain is placed very close to entrance of the thin channel.

consecutive events: approach of the chain to the entrance of the thin channel, escape of the chain over the entropic barrier at the entrance of the thin channel, and motion of the entire chain across the thin channel. All three events are associated with characteristic time scales which depend on the chain length, N.

Whereas τ_{app} and τ_{act} decrease with N, τ_{cross} increases with N. For the values of E_{av} used in the simulations, τ_{act} and τ_{cross} become equal to each other at N_{cr}, a crossover value of N. Since τ_{cross} and τ_{act} display opposite dependences with respect to N, $\tau_{act} > \tau_{cross}$ for $N < N_{cr}$ whereas $\tau_{cross} > \tau_{act}$ for $N > N_{cr}$. Therefore, N_{cr} defines a transition from an activation-dominated regime for $N < N_{cr}$ to a crossing-dominated regime for $N > N_{cr}$. As a result, $v_{transit}$ first increases with N in the activation-dominated regime, attains a maximum at N_{cr}, and then decreases with further increase in N. This implies that the dependence of $v_{transit}$ on N can be governed by more than one physical mechanism. The behavior reported here complements previous studies,[5,9] which generally focused on how only one physical mechanism determines the dependence of $v_{transit}$ on N.

We have also shown that N_{cr} can be changed by varying E_{av}. By reducing E_{av}, we found that N_{cr} shifts to larger values of N, which means that the activation-dominated regime spans a larger range of N as compared to the crossing-dominated regime. At low enough fields, one could have a situation where the activation event dominates over the crossing event for the entire range of relevant chain lengths. In such a situation, values of τ_{cross} would always be smaller than τ_{act}, and $v_{transit}$ would increase with N. This provides us with a better understanding of Han and Craighead's experiments, where the crossing event would take place but its role is never manifested because τ_{cross} is always less than τ_{act}. We note that the transit velocity we calculate may not be the same as the average transit velocity through an array of narrow constrictions. If the average transit velocity also exhibits a nonmonotonic dependence on N under some conditions, then some polymers with different lengths will move at the same speed and separation will be compromised.

These ideas can also be used to explain some aspects of polymer translocation through nanopores, where the activation mechanism is expected to be limited to end-activation due to the small size of the pore and the finite persistence length of the DNA or RNA molecule. Since end-activation is independent of N, $v_{transit}$ would now decrease with N since τ_{cross} depends inversely on N. Our results for the case of an end-activated transit seem to support this view for both 2D and 3D channels.

With these simulations, we have been able to establish a connection between the two problems of polymer electrophoresis in the entropic trapping device and polymer translocation through nanopores. It has been pointed out previously[19] that both problems involve a polymer chain crossing a free energy barrier. By analyzing our results, not only have we been able to verify this picture but also we have identified specific processes which determine polymer transport and which give rise to differences in the chain length dependence of the transit velocity for the two problems. Our work may also serve as a starting point for further studies which include additional physical phenomena (e.g., excluded volume, electrostatic, and hydrodynamic interactions, polymer−wall attraction) and aim to find conditions under which electrophoretic separations are optimized.

Acknowledgment. We are grateful to Prof. David Morse for insightful discussions on this subject. This material is based upon work supported in part by the U.S. Army Research Laboratory and the U.S. Army Research Office under Grant W911 NF-04-1-0265. Our work was also supported in part by the Army High Performance Computing Research Center under the auspices of the Department of the Army, Army Research Laboratory (ARL) under Cooperative Agreement DAAD19-01-2-0014. The content does not necessarily reflect the position or policy of the government, and no official endorsement should be inferred.

References and Notes

(1) Viovy, J.-L. *Rev. Mod. Phys.* **2000**, *72*, 813.
(2) Slater, G. W.; Guillouzic, S.; Gauthier, M. G.; Mercier, J.-F.; Kenward, M.; McCormick, L. C.; Tessier, F. *Electrophoresis* **2002**, *23*, 3791.
(3) Lehninger, A. L.; Nelson, D. L.; Cox, M. M. *Principles of Biochemistry*; Worth Publishers: New York, 1993.
(4) Meller, A. *J. Phys.: Condens. Matter* **2003**, *15*, R581.
(5) Han, J.; Turner, S. W.; Craighead, H. G. *Phys. Rev. Lett.* **1999**, *83*, 1688.
(6) Han, J.; Craighead, H. G. *J. Vac. Sci. Technol. A* **1999**, *17*, 2142.
(7) Han, J.; Craighead, H. G. *Science* **2000**, *288*, 1026.
(8) Han, J.; Craighead, H. G. *Anal. Chem.* **2002**, *74*, 394.
(9) Kasianowicz, J. J.; Brandin, E.; Branton, D.; Deamer, D. W. *Proc. Natl. Acad. Sci. U.S.A.* **1996**, *93*, 13770.
(10) Meller, A.; Nivon, L.; Branton, D. *Phys. Rev. Lett.* **2001**, *86*, 3435.
(11) Li, J.; Gershow, M.; Stein, D.; Brandin, E.; Golovchenko, J. A. *Nat. Mater.* **2003**, *2*, 611.
(12) Chen, P.; Gu, J.; Brandin, E.; Kim, Y.-R.; Wang, Q.; Branton, D. *Nano Lett.* **2004**, *4*, 2293.
(13) Fan, R.; Karnik, R.; Yue, M.; Li, D.; Majumdar, A.; Yang, P. *Nano Lett.* **2005**, *5*, 1633.
(14) Storm, A. J.; Storm, C.; Chen, J.; Zandbergen, H.; Joanny, J.-F.; Dekker, C. *Nano Lett.* **2005**, *5*, 1193.
(15) Storm, A. J.; Chen, J. H.; Zandbergen, H. W.; Dekker, C. *Phys. Rev. E* **2005**, *71*, 051903.
(16) Sung, W.; Park, P. J. *Phys. Rev. Lett.* **1996**, *77*, 783.
(17) Park, P. J.; Sung, W. *J. Chem. Phys.* **1999**, *111*, 5259.

(18) Lubensky, D. K.; Nelson, D. R. *Biophys. J.* **1999**, *77*, 1824.
(19) Sebastian, K. L.; Paul, A. K. R. *Phys. Rev. E* **2000**, *62*, 927.
(20) Sebastian, K. L. *Phys. Rev. E* **2000**, *61*, 3245.
(21) Sebastian, K. L. *J. Am. Chem. Soc.* **2000**, *122*, 2972.
(22) Kumar, K.; Sebastian, K. L. *Chem. Phys. Lett.* **2002**, *359*, 101.
(23) Ambjörnsson, T.; Apell, S. P.; Konkoli, Z.; Di Marzio, E. A.; Kasianowicz, J. J. *J. Chem. Phys.* **2002**, *117*, 4063.
(24) Muthukumar, M. *J. Chem. Phys.* **2003**, *118*, 5174.
(25) Slonkina, E.; Kolomeisky, A. B. *J. Chem. Phys.* **2003**, *118*, 7112.
(26) Flomenbom, O.; Klafter, J. *Phys. Rev. E* **2003**, *68*, 041910.
(27) Kong, C.; Muthukumar, M. *J. Chem. Phys.* **2004**, *120*, 3460.
(28) Matsuyama, A. *J. Chem. Phys.* **2004**, *121*, 8098.
(29) Nixon, G. I.; Slater, G. W. *Phys. Rev. E* **1996**, *53*, 4969.
(30) Tessier, F.; Labrie, J.; Slater, G. W. *Macromolecules* **2002**, *35*, 4791.
(31) Chen, Z.; Escobedo, F. A. *Mol. Simul.* **2003**, *29*, 417.
(32) Streek, M.; Schmid, F.; Duong, T. T.; Ros, A. *J. Biotechnol.* **2004**, *112*, 79.
(33) Kong, C. Y.; Muthukumar, M. *Electrophoresis* **2002**, *23*, 2697.
(34) Kim, S. H.; Panwar, A. S.; Kumar, S.; Ahn, K. H.; Lee, S. J. *J. Chem. Phys.* **2004**, *121*, 9116.
(35) Chen, C.-M. *Physica A* **2005**, *350*, 95.
(36) Rabin, Y.; Tanaka, M. *Phys. Rev. Lett.* **2005**, *94*, 148103.
(37) Chern, S.-S.; Cárdenas, A. E.; Coalson, R. D. *J. Chem. Phys.* **1999**, *115*, 7772.
(38) Tian, P.; Smith, G. D. *J. Chem. Phys.* **2003**, *119*, 11475.
(39) Loebl, H. C.; Randel, R.; Goodwin, S. P.; Matthai, C. C. *Phys. Rev. E* **2003**, *67*, 041913.
(40) Randel, R.; Loebl, H. C.; Matthai, C. C. *Macromol. Theory Simul.* **2004**, *13*, 387.
(41) Lansac, Y.; Maiti, P. K.; Glaser, M. A. *Polymer* **2004**, *45*, 3099.
(42) Kantor, Y.; Kardar, M. *Phys. Rev. E* **2004**, *69*, 021806.
(43) Manning, G. S. *J. Chem. Phys.* **1981**, *85*, 1506.
(44) Smisek, D. L.; Hoagland, D. A. *Science* **1990**, *248*, 1221.
(45) Arvanitidou, E.; Hoagland, D. A. *Phys. Rev. Lett.* **1991**, *67*, 1464.
(46) Bousse, L.; Cohen, C.; Nikiforov, T.; Chow, A.; Kopf-Sill, A. R.; Dubrow, R.; Parce, J. W. *Annu. Rev. Biophys. Biomol. Struct.* **2000**, *29*, 155.
(47) Baumgartner, A.; Muthukumar, M. *J. Chem. Phys.* **1987**, *87*, 3082.
(48) Muthukumar, M.; Baumgartner, A. *Macromolecules* **1989**, *22*, 1937.
(49) Muthukumar, M.; Baumgartner, A. *Macromolecules* **1989**, *22*, 1941.
(50) Hoagland, D. A.; Muthukumar, M. *Macromolecules* **1992**, *25*, 6696.
(51) Slater, G. W.; Wu, S. Y. *Phys. Rev. Lett.* **1995**, *75*, 164.
(52) Nixon, G. I.; Slater, G. W. *J. Chem. Phys.* **2002**, *117*, 4042.
(53) Chern, S.-S.; Coalson, R. D. *J. Chem. Phys.* **1999**, *111*, 1778.
(54) Rousseau, J.; Drouin, G.; Slater, G. W. *Phys. Rev. Lett.* **1997**, *79*, 1945.
(55) Volkmuth, W. D.; Duke, T.; Austin, R. H.; Cox, E. C. *Proc. Natl. Acad. Sci. U.S.A.* **1992**, *92*, 6887.
(56) Turner, S. W.; Perez, A. M.; Lopez, A.; Craighead, H. G. *J. Vac. Sci. Technol. B* **1998**, *16*, 3835.
(57) Panwar, A. S.; Kumar, S. *J. Chem. Phys.* **2005**, *122*, 154902.
(58) Grassia, P.; Hinch, E. J. *J. Fluid Mech.* **1996**, *308*, 255.
(59) Andre, P.; Long, D.; Ajdari, A. *Eur. Phys. J. B* **1998**, *4*, 307.
(60) Fixman, M. *J. Chem. Phys.* **1978**, *69*, 1527.
(61) Morse, D. C. *Adv. Chem. Phys.* **2004**, *128*, 65.
(62) Streek, M.; Schmid, F.; Duong, T. T.; Anselmetti, D.; Ros, A. *Phys. Rev. E* **2005**, *71*, 011905.

MA051041O